Dalton Transactions

Accepted Manuscript

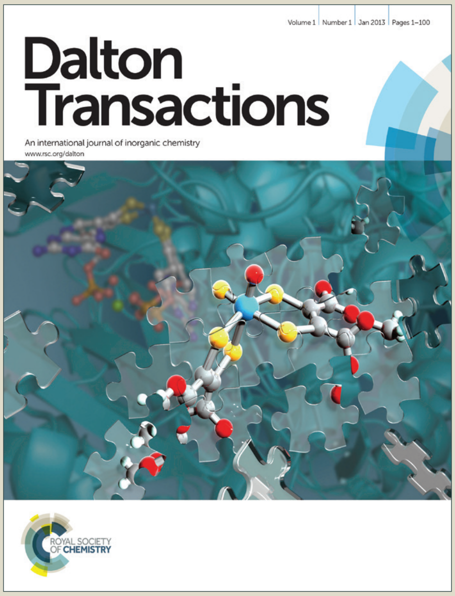

ROYAL SOCIETY OF CHEMISTRY

www.rsc.org/dalton

Journal Name

Dalton Transactions

Dynamic Article Links ►

Cite this: DOI: 10.1039/c0xx00000x

www.rsc.org/xxxxxx

ARTICLE TYPE

Synthesis, characterization and insights into stable and well organized hexagonal mesoporous zinc-doped alumina as promising metathesis catalysts carrier

Abdelnasser Abidli,[a,b] Safia Hamoudi,[a,b] and Khaled Belkacemi*[a,b]

Received (in XXX, XXX) Xth XXXXXXXXX 20XX, Accepted Xth XXXXXXXXX 20XX

DOI: 10.1039/b000000x

A series of highly ordered hexagonal mesoporous alumina and zinc-modified mesoporous alumina are synthesized *via* a sol-gel method through an evaporation-induced self-assembly process using Pluronic F127 as nonionic templating agent and several aluminum precursors. The process was mediated using several carboxylic acids along with hydrochloric acid in ethanol. Successful impregnation of $ZnCl_2$ was achieved while maintaining the ordered structure. The surface and textural properties of the materials have been investigated. N_2-physisorption analysis revealed a BET surface area of 394 m^2/g and a pore volume around 0.55 cm^3/g. Moreover, small-angle XRD diffraction patterns highlighted the well-organized hexagonal structure even upon the incorporation of zinc chloride. The organized-structure arrangement was further confirmed by transmission electron microscopy (TEM) analysis. The Zn/Al composition of the final materials was confirmed by EDX and XPS analysis, and the zinc amount incorporated was analyzed by ICP. Furthermore, the surface modification with zinc chloride impregnation was analyzed by XPS, ^1H- and ^{27}Al MAS-NMR and FTIR spectroscopy techniques. In addition, the effects of synthetic conditions and the mechanism of the mesostructure formation was explored. The catalytic activity of several methyltrioxorhenium (MTO)-based catalysts supported on these hexagonal mesoporous alumina materials was tested for methyl oleate self-metathesis. The results showed improved kinetics using hexagonal alumina in comparison to those using wormhole-like alumina counterparts. This behavior could be attributed to better mass transfer features of hexagonal mesoporous alumina. The prepared materials with desirable pore size and structure are suitable candidates as catalyst supports for metathesis of bulky functionalized olefins and other catalytic transformations due to their enhanced Lewis acidity and more uniform pore networks favoring enhanced and selective mass transfer phenomena.

Introduction

Ordered materials attracted an enormous attention of many research groups focusing on the enhancement of several heterogeneous catalysts activities and selectivity. This was carried out by the improvement of the surface organization and porous network uniformity of these materials.[1-7] These textural aspects offered advantageous alternatives towards desired shape-selective catalysis which are governed by mass transfer phenomena. These phenomena can be tuned by controlling the porosity and the surface homogeneity.[8] Moreover, this key point is more critical when selectivity is an issue, dealing with bulky molecules that undergo both intra- and inter-molecular reactions. Despite the increasing progress that has been achieved since the first synthesis of hexagonally ordered mesoporous silica,[9-11] the synthesis of ordered materials for catalytic applications still remains as a hot research topic. Indeed, various organized mesoporous siliceous and non-siliceous materials were targeted, among them; cubic MCM-41and MCM-48,[12] SBA-15[11] and KIT-6,[13] in addition to ordered mesoporous carbon (CMK-1 and CMK-3),[14, 15] nobia,[16, 17] titania,[17] zirconia,[17] tantalum oxide[18] and other several non-siliceous interesting ordered mesoporous metal oxides[19] and hybrid materials.[20]

Ordered mesoporous alumina (OMA) has been one of the challenging non-siliceous organized materials to synthesize.[21, 22] Niesz *et al.*[23] reported a Pluronic P123-templated sol-gel synthesis of OMA where the synthesis was performed at 40 °C affording high BET surface and narrow pore size distribution. Liu *et al.*[24] reported a nanocasting synthesis templated by mesoporous CMK-3 carbon. A Pluronic F127-templated synthesis of OMA was also reported by Yuan *et al.*[25] Recently, Wu *et al.*[26] reported an efficient OMA synthesis using inexpensive aluminum nitrate at 30 °C. OMA with relatively large mesopores have been obtained using a swelling agent in a Pluronic P123-templated synthesis. Along with high surface area and pore size and uniform mesoporous network, great efforts have been also focused on achieving thermally and hydrothermally stable crystalline framework walls of OMA.[4, 24, 25] Moreover this feature can help the material to maintain large surface area even after thermal treatment at high temperatures.[27]

[a] *Department of Soil Sciences and Agri-Food Engineering, Laval University. G1V 0A6, Quebec city, Quebec, Canada. Fax: (418) 656 3723; Tel: (418) 656 2131 ext: 6511; E-mail: khaled.belkacemi@fsaa.ulaval.ca*
[b] *Centre in Green Chemistry and Catalysis (CGCC). H3A 0B8, Montreal, Quebec, Canada.*

† Electronic Supplementary Information (ESI) available: See DOI: 10.1039/b000000x/

In order to establish a versatile and cost-effective preparation of OMA materials, many approaches have been investigated. These studies revealed the importance of many key-control factors in order to overcome limitations over ordered mesoporous network formation. Therefore, the effect of inorganic precursors-template ratio was investigated.[8] Furthermore, many process parameters were deeply investigated among them, the complexation effect of anions and hydro-carboxylic acid and organic-inorganic interface protectors and template-assistants during aging process,[25, 27-30] synthetic routes,[31] swelling agents and co-solvents,[32] salt-like effect of water and acid concentration,[33] the pH of the synthesis medium and nature of pH adjustor,[25, 34] as well as the calcination temperature.[25]

The particular acidic properties of the alumina surface attributed to Lewis-acid aluminum species and Brønsted-acid hydroxyl groups, promoted significantly the incorporation of several metals and other metal oxides on alumina. Frequently, OMA modification and synthesis under high thermal conditions led to partial or complete loss of the mesoporous hexagonal arrangement.[35] Therefore, doping metals and metal oxides on OMA and preserving the well-ordered 2D-hexagonal mesostructure is a challenging procedure. In this perspective, various elements were supported on OMA and simultaneously maintaining the organized structure. For instance, Ni, Mg, Fe, Cr, Cu, Ce, La, Y, Ca and Sn were successfully supported on OMA.[35, 36] Si-, Ce-, and Zr-doped OMA,[37] Ce–Zr-Co-doped OMA,[38, 39] Cu/Ce-OMA,[40] La-doped OMA[41] and noble metals-doped OMA (Pt, Ag and Pd)[42] were also prepared. Similarly, OMA-supported metal oxides such as; MgO, CaO, TiO_2, and Cr_2O_3[35] and ordered titania-alumina mixed oxides[43] were also obtained. In addition, to prevent OMA collapse, the metal-modified OMA were obtained with uniform metal dispersion. These materials presented high catalytic activities for various reactions including carbon dioxide reforming of methane,[44] hydrogen production,[45] CO oxidation,[42] thiophene hydrodesulfurization[46] and methanol dehydration.[47]

Catalytic metathesis reaction could be one of these applications that can benefit from the ordered mesostructure network of alumina and modified-alumina, especially when *trans*- or *cis*-selectivity is critical and highly desired.

Actually, metathesis reaction is an efficient transformation offering direct access to industrially important products from oleochemicals in one reaction step. Metathesis of fats and oils is a clean catalytic and atom efficient reaction with no by-product formation.[48] It is a transalkylidenation reaction involving substituents rearrangement of molecules containing C=C bonds resulting in exchange of alkylidene fragments.

A number of catalysts have been developed for metathesis of functional olefins. The most active homogeneous catalysts developed are transition metals-based alkylidene complexes. Grubbs, Hoveyda-Grubbs, Schrock catalysts are the most successful among them and they are commercially available.[49] These homogeneous catalysts are active and compatible with a wide range of functional groups. However, they are expensive and often non-reusable. Typical heterogeneous catalysts for metathesis are based on transition metal complexes in presence of co-catalysts or promoters. Traditional catalytic systems consist of metal chlorides, oxides and oxychlorides, often based on Mo, W, and Re and less commonly based on Os, Ir and Ti with co-catalysts which are generally Lewis acids or organometallic compounds of non-transition metals like Al and Sn.[50]

Methyl oletate was used as a model molecule for the studies on metathesis of functionalized bulky olefins contained in vegetable. The most widely used heterogeneous catalysts for methyl oleate metathesis were Re_2O_7 supported on alumina and silica-alumina materials.[50, 51] However these catalysts require the use of toxic tin-based promoters and additives such as Bu_4Sn to increase the catalyst reactivity. The presence of tin also hinders the catalyst regeneration due to the deposed SnO_2 species on the catalyst surface, formed during each recycling process which reacts with the active Re oxide.[52]

Owing to the above limitations of Re_2O_7-based heterogeneous catalysts, the need for alternative approaches without using toxic molecules arises. Methyltrioxorhenium (MTO) was found to be an active organorhenium complex for metathesis catalysis without the use of toxic promoter.[53, 54] We have demonstrated recently that zinc chloride-modified wormhole-like mesoporous alumina exhibited higher metathesis activity comparing to alumina supports.[55-57] Furthermore, we hypothesized that a well structurally organized alumina would be more suitable, expecting to improve the catalyst performance for the functionalized olefin metathesis reaction.

In the present work, we report the synthesis of well-organized hexagonal $ZnCl_2$-modified alumina. The effects of aluminum precursor and interfacial protectors (CA: carboxylic acids) on mesophase formation were investigated using simple carboxylic acids to prepare a series of ordered modified-alumina. A comprehensive mechanism of mesopores formation using carboxylic acids is proposed. The catalytic activity for methyl oleate self-metathesis using methyltrioxorhenium (MTO) supported on these well-ordered Zn-modified Al_2O_3 was investigated for the first time on this material and comparison with wormhole-like alumina is also discussed.

Experimental section

Chemicals and reagents

Pluronic F127 ($EO_{106}PO_{70}EO_{106}$, MW = 12 600), aluminum isopropoxide $Al(OPr^i)_3$ (≥98.0%), aluminum-tri-*sec*-butoxide $Al(OBu^s)_3$ (97.0%), citric acid (≥99.5%), L-(+)-tartaric acid (≥99.5 %), fumaric acid (≥99.5 %), oxalic acid (>99.0%), maleic acid (≥99.0%), acetic acid (≥99.7%) and zinc chloride ($ZnCl_2$, 99.9%) were purchased from Sigma-Aldrich Canada (Oakville, ON, Canada). Aluminum tri-*tert*-butoxide $Al(OBu^t)_3$ (97.0%) was purchased from VWR International (Mississauga, ON, Canada). Aluminum nitrate nonahydrate $Al(NO_3)_3{\bullet}9H_2O$ (99.9%), hydrochloric acid (HCl, 36.5-38 wt%) and malonic acid (≥99.0%) were purchased from Acros Organics (Morris Plains, NJ, USA). Cyclohexane (99.9%), hexane (99.0%), and ethanol (99.9%) were purchased from Fisher Scientific (Ottawa, Ontario, Canada). All reagents were used as received without further purification. All gases used were provided by Praxair at a purity of at least 99.995%

Alumina and modified-alumina synthesis

Synthesis of well-ordered hexagonal mesoporous alumina (meso-Al_2O_3)

Highly ordered hexagonal mesoporous alumina (Al_2O_3-meso) materials were synthesized through an extended sol-gel process associated with nonionic block copolymer as a directing agent, in a similar procedure described by Yuan *et al.*[25] Their synthesis was screened under different conditions (carboxylic acid, aluminum precursor and calcination temperature). Typically, Pluronic F127 (2.17 g) was dissolved in anhydrous ethanol (20 mL) under stirring at room temperature. Then, the investigated carboxylic acid (2.6 mmol) was added. The pH of the solution was adjusted below 2 by adding hydrochloric acid (1.0-1.5 mL), giving a clear solution. The investigated aluminum-precursor (10 mmol) was subsequently added under vigorous stirring. The mixture was then covered with polyethylene film, and left under stirring at room temperature for 5 h. The solvent was removed slowly in a drying oven at 60 °C and aged for 48h. The obtained solid was heated from room temperature to 400 °C with a slow ramping rate (1 °C/min), and calcined for 4 h in air. The obtained Al_2O_3–meso material was calcined further at higher temperatures (up to 1100 °C) at ramping rate of 10 °C/min for 1 h in air (2 h for 600-700 °C).

Zinc chloride ($ZnCl_2$) modification of ordered alumina (Al_2O_3)

The modification of ordered alumina with $ZnCl_2$ was carried out using the procedure reported in our previous works.[55-57] In a typical synthesis, meso-Al_2O_3 (2.0 g) was suspended in ethanol (20 mL) under stirring at room temperature. Zinc chloride (334 mg, 2.45 mmol) was dissolved in ethanol (10 mL) by applying a 30 s vortex mixing. The addition of $ZnCl_2$ solution to meso-Al_2O_3 suspension was carried out drop wise under stirring. The mixture was kept under stirring at room temperature for 24 h in air, allowing a complete evaporation of ethanol. The obtained dried sample was heated from room temperature to 400 °C with a ramping rate of 2 °C/min, and then calcined for 4 h in air, providing $ZnCl_2$-modified Al_2O_3–meso with optimized Al:Zn molar ratio of 8:1 as reported in our previous works.[55-57]

Catalytic activity evaluation and GC analysis of the reaction products

The synthesized catalysts were tested for methyl oleate self-metathesis in hexane under controlled dry atmosphere at 45 °C for 3h. Aliquots were taken at different time intervals. The reaction was monitored by GC analysis using dodecane as internal standard. The products were identified using pure standards and GC-MS analysis as reported in our previous works.[55-57]

Characterization of the materials and the surface sites

The prepared alumina and zinc chloride-modified alumina materials were characterized using Powder X-ray diffraction (XRD) and N_2 physisorption. Also transmission electron microscopy (TEM), scanning electron microscopy (SEM) and Energy-dispersive X-ray (EDX) spectroscopy measurements were performed. The synthesized materials were also characterized using X-ray photoelectron spectroscopy (XPS), inductively coupled plasma optical emission spectroscopy (ICP-OES), ^{1}H and ^{27}Al magic angle spinning nuclear magnetic resonance (MAS NMR) techniques, as well as Fourier transform infrared (FTIR) spectroscopy.

Powder X-ray diffraction (XRD) measurements

The crystal structures of the calcined samples were analyzed by XRD using a an Ultima III Rigaku monochromatic diffractometer (Model D/MAX-2200, with CuKα radiation source (λ=1.54059 Å) operated at a voltage of 40 kV and a current of 44 mA. Small angle XRD measurements were performed over the 2θ angle range of 0.6-6° at a scanning rate of 0.5°/min. The different crystal phases were identified by wide angle XRD measurements. The patterns were collected from 10° to 80° at a speed of 5.0°/min.

Brunauer–Emmett–Teller (BET) surface area measurements

The textural properties and surface analysis of calcined samples were performed by nitrogen adsorption/desorption isotherms. The samples were initially out-gassed under vacuum (10^{-4} Torr) at 250-300 °C during 12 h. Then, the multipoint BET surface area measurement was carried out using a volumetric adsorption analyzer (Model Autosorb-1, Quantachrome Instruments, Boyton Beach, FL) at liquid nitrogen temperature -196 °C (77 K). The specific surface area was evaluated using the Brunauer–Emmett–Teller (BET) method. Total pore volume was estimated from the amount adsorbed at the relative pressure $P/P_0 = 0.990$ single point. Pore size distribution curves were calculated using the desorption branch of the N_2-adsorption/desorption isotherms and the Barrett-Joyner-Halenda (BJH) method as reported in the literature for this type of materials.[58-60]

Transmission electron microscopy (TEM) studies

The pore size and morphology were examined by transmission electron microscopy (TEM). The micrographs were taken from a JEM-1230 electron microscope (JEOL, Japan) equipped with a lanthanum hexaboride (LaB_6) thermionic emission source, operated at an acceleration voltage up to 80 kV, using Gatan dual-view multiscan camera. For TEM observations, the powdered samples were dispersed in methanol and sonicated for 10 min. A suspension drop of the obtained solution (5 µL) was then placed uniformly onto a Formvar film coated nickel grid (200 meshes) and it was allowed to dry in air at room temperature before analysis.

Microstructural characterizations SEM/EDX

The microstructure, morphology and elemental composition of the synthesized materials were determined using scanning electron microscopy (SEM) along with energy dispersive X-ray spectrometry (EDX). Before analysis, powdered samples were dispersed on a copper grid (300 mesh) coated with a Lacey amorphous carbon film. The samples were deposited by cathodic sputtering in vacuum chamber (100 mTorr), using an Au/Pd thin film to make the surface electrically conductive for better sensitivity and higher imaging resolution. The characterization was carried out on a JEOL model JSM-840A scanning electron microscope equipped with an energy-dispersive X-ray (EDX) spectrometer operating at an accelerating voltage of 15 kV using secondary electron mode at high vacuum (10^{-6} Torr). EDX spectra of the particles were collected using a single-point quantitative analysis taken from several random areas of the sample. SEM images were acquired using OrionTM software at different magnifications (X 350-3000). The EDX signals were obtained by focusing a high energy electron beam on the particles and accumulating the spectra within an acquisition time of 60 s using Spirit^{TM} Bruker AXS Microanalysis software. Average atomic ratio of the present elements was calculated from several EDX spectra at different points of the prepared sample.

Inductively coupled plasma optical emission spectrometry (ICP-OES) analysis

The actual Al/Zn atomic ratio and the Re loading in the prepared catalyst supports was determined by ICP-OES using a Perkin-Elmer Optima 4300DV ICP-emission spectrometer with radial plasma viewing. For analysis, 10 mg of sample were digested with 5 mL of *aqua regia* (nitro-hydrochloric acid) solution. After 24 h, the solution was filled up to 50 mL with deionized water for sample dilution to perform ICP experiments. Measurements from emission spectra for the dissolved species were conducted using calibration curves of a series of Al, Zn and Re standard solutions. The experimental ICP metal composition values were compared to the expected Al/Zn atomic ratio for each sample.

X-ray photoelectron spectroscopy (XPS) measurements

Identification of material surface species and their oxidation/coordination states was achieved by means of XPS analysis. XPS spectra were recorded on an AXIS ULTRA from Kratos Analytical (Manchester, UK) equipped with a double X-ray source for non-monochromatic Al-Mg (Kα) X-ray irradiation, a monochromatic Al (Kα) X-ray irradiation source (1486.6 eV), and an electrostatic analyzer of large radius. The base pressure in the UHV XPS chamber was 5 10^{-10} Torr. All spectra were acquired with the Al monochromatic source at room temperature operated at 300 W. The working pressure in the analyzing chamber was less than 10^{-7} Torr. The survey spectrum used to determine the elementary apparent composition was recorded with pass analyzer energy of 160 eV and an energy step of 1 eV, using lenses in the hybrid mode, which maximizes sensitivity.[61, 62] The detailed spectra were obtained with pass energy of 20 or 40 eV, and an energy step of 50 or 100 meV. The charge neutralizer was used for charge compensation of the non-conducting samples. The binding energies were corrected for charge shifts, with the use of the C1*s* set at 285 eV peak as internal reference.[63] The uncertainty in the reported binding energy (BE) values is ±0.1 eV. The survey spectra were recorded in the binding energy range 0–1150 eV, and detailed spectra were recorded for O1s, Zn2*p*, Zn Auger L2M45 M45, Cl2*p* and Al2*p*. Curve fitting and deconvolution were performed using mixed Gaussian/Lorentzian line shapes after a Shirley-type background removal by using the CasaXPS 2.3.15 software.[64]

^{1}H -MAS NMR measurements

Catalyst framework was investigated by solid-state NMR spectroscopy. ^{1}H-MAS NMR spectra were recorded on a Bruker AVANCE 300 (Bruker BioSpin Ltd.) wide bore NMR spectrometer equipped with superconducting magnet of 7.1 Tesla using a conventional 4mm-broadband resonance magic angle spinning MAS probehead at operating Larmor frequencies of 300.1 MHz. The dehydrated samples were quickly packed into a 4 mm-zirconia (ZrO_2) rotor, and then the spectra were acquired at room temperature at a typical spinning rate of 10 kHz at the magic angle. Single pulse excitation^{1}H-NMR experiments were performed for Al_2O_3-meso and the $ZnCl_2$-modified Al_2O_3-meso using a 90° pulse length of 2.25 μs, an acquisition time of 30 ms, and a recycle delay between scans of 60 s. Eight scans were collected for each ^{1}H-MAS-NMR spectrum. All the corresponding chemical shift values were referenced to tetramethylsilane (TMS) signal (0.0 ppm in a spinning rotor).

^{27}Al-MAS NMR investigations

The form, coordination state and environment of aluminum, as well as the surface and intrinsic Lewis acidic site concentrations were studied by means of ^{27}Al solid-state magic-angle spinning (MAS) NMR spectroscopy measurements. The experiments were conducted on a Bruker Avance 300 (7.1 T) instrument. ^{27}Al-MAS-NMR spectra were obtained using a high-speed broadband MAS-probe with an outer diameter of 4 mm, and rotated around the Magic Angle at a rate of 10 kHz controlled within ±2 Hz using a Bruker MAS-controller, with an acquisition time of 15.4 ms. The system was operated at a resonance frequency of 78.1 MHz for ^{27}Al nuclei. All spectra were obtained at room temperature. For the 1D- spectrum measurements, a short single excitation $\pi/10$ pulse of 0.6 μs was applied. The small flip angle of the ^{27}Al pulse was advantageously used to improve signal intensity quantification of the quadrupole nucleus.[65] The relaxation time was set at 250 ms, and 2000 scans were recorded. The ^{27}Al-NMR ppm scale was referenced to $Al(NO_3)_3•9H_2O$ by adjusting the signal to 0 ppm.[66]

Fourier transform infrared (FTIR) spectroscopy studies

FTIR investigations of the mesophase formation pathway were carried out in a Nicolet Magna 850 FTIR spectrometer (Thermo Fisher Scientific Inc.) equipped with a liquid nitrogen-cooled MCT detector in absorbance mode under static conditions. Before analysis, the samples were degassed under vacuum (10^{-4} Torr) at 250 °C overnight. FTIR spectra were recorded at room temperature in the mid-IR spectral range; 400-4000 cm^{-1} region at 4 cm^{-1} resolution accumulating 128 scans. ATR-FTIR data acquisition and manipulation were performed with Omnic^{TM} software (v. 6.1) and presented as absorbance. Spectra were obtained using a 45° trough-style sample holder with a zinc selenide (ZnSe) internal reflection element (56 mm×10 mm×3 mm) (PIKE Technologies, Inc) yielding nine internal reflections, while deconvolution of the IR spectra was carried out using the ORIGIN software (OriginLab Corporation, Northampton, MA).

Results and discussion

Material characterizations

Physisorption analysis and material textural properties

Aluminum-tri-*sec*-butoxide was used as aluminum precursor for the synthesis of conventional wormhole-like alumina as reported in our previous work.[55-57] Therefore, different hexagonal OMA materials were prepared using the same precursor in the presence of several, inexpensive mono-, di- and tri-carboxylic acids. Table1 shows the textural properties of these materials.

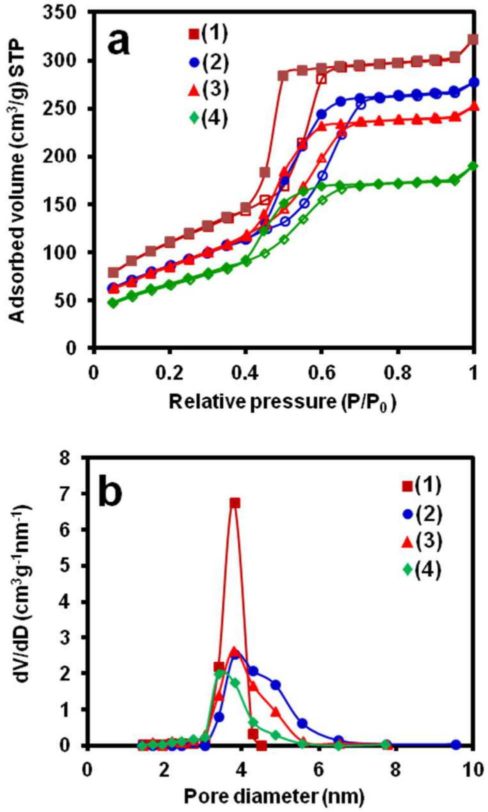

Fig. 1 (a) Nitrogen adsorption–desorption isotherms and (b) pore size distributions of the prepared OMA samples: (1) Al_2O_3-tartaric, (2) Al_2O_3-fumaric, (3) Al_2O_3-oxalic and (4) Al_2O_3-maeilc acid, synthesized using $Al(OBu^s)_3$ and calcined at 400 °C.

Figure 1 shows the nitrogen adsorption-desorption isotherms of hexagonal OMA synthesized using different carboxylic acids. All isotherms are IV-type and exhibit H1-type hysteresis loops. These isotherms display well-known patterns of organized mesoporous network containing cylindrical channels. Moderate to relatively large BET surface area (up to 394 m^2/g), pore volume (up to 0.55 cm^3/g) and uniform narrow pore distribution with average pore size of 3.4-4.9 nm were obtained (Table 1).

No significant difference was observed with the investigated carboxylic acids (see also Figure S1 in the Supporting Information) which could be attributed to their similar coordination abilities with Al centers *via* monodentate or bridging bidentate modes during the mesophase formation process.[67] Moreover, similar BET surface area and pore volume were obtained using different aluminum precursors (See Table 1) showing also typical type-IV curves with H1-hysteresis (Figure 2) characteristic for mesoporous solids.[68]

Table 1 Textural properties of the prepared hexagonally OMA and zinc chloride-modified OMA obtained by means of N_2 adsorption–desorption isotherms.

Alumina	Acid	Aluminum precursor	S_{BET}[a] (m^2/g)	V_P[b] (cm^3/g)	D_P[c] (nm)	$ZnCl_2$-Modified Al_2O_3[d]	S_{BET}[a] (m^2/g)	V_P[b] (cm^3/g)	D_P[c] (nm)
Al_2O_3-1	Citric	$Al(OBu^s)_3$	362	0.46	3.4	$ZnCl_2$-Al_2O_3-1	316	0.44	3.8
Al_2O_3-2	Tartaric	$Al(OBu^s)_3$	394	0.49	3.8	$ZnCl_2$-Al_2O_3-2	154	0.26	3.8
Al_2O_3-3	Fumaric	$Al(OBu^s)_3$	313	0.43	3.9	$ZnCl_2$-Al_2O_3-3	214	0.31	3.8
Al_2O_3-4	Oxalic	$Al(OBu^s)_3$	317	0.39	3.8	$ZnCl_2$-Al_2O_3-4	ND[e]	ND	ND
Al_2O_3-5	Maleic	$Al(OBu^s)_3$	319	0.31	3.4	$ZnCl_2$-Al_2O_3-5	ND	ND	ND
Al_2O_3-6	Malonic	$Al(OBu^s)_3$	298	0.29	3.4	$ZnCl_2$-Al_2O_3-6	ND	ND	ND
Al_2O_3-7	Acetic	$Al(OBu^s)_3$	378	0.55	3.8 and 4.9	$ZnCl_2$-Al_2O_3-7	ND	ND	ND
Al_2O_3-8	Citric	$Al(OBu^t)_3$	300	0.53	5.5	$ZnCl_2$-Al_2O_3-8	239	0.41	4.9
Al_2O_3-9	Tartaric	$Al(OBu^t)_3$	324	0.59	5.6	$ZnCl_2$-Al_2O_3-9	257	0.44	5.6
Al_2O_3-10	Citric	$Al(OPr^i)_3$	321	0.24	4.9	$ZnCl_2$-Al_2O_3-10	241	0.38	3.8 and 4.9
Al_2O_3-11	Tartaric	$Al(OPr^i)_3$	289	0.46	5.6	$ZnCl_2$-Al_2O_3-11	190	0.39	5.7
Al_2O_3-12	Citric	$Al(NO_3)_3 \cdot 9H_2O$	337	0.30	3.8	$ZnCl_2$-Al_2O_3-12	139	0.40	3.8 and 6.5
Al_2O_3-13	Tartaric	$Al(NO_3)_3 \cdot 9H_2O$	293	0.58	3.8	$ZnCl_2$-Al_2O_3-13	222	0.46	3.8

[a] BET specific surface area (m^2/g); [b] BJH pore volume (cm^3/g) determined at $P/P_0 = 0.997$; [c] BJH average pore diameter (nm); [d] Al:Zn atomic ratio of 8:1 determined by ICP-OES analysis; [e] ND: Not determined.

However, the OMA prepared with $Al(OBu^t)_3$ and $Al(OPr^i)_3$ afforded larger pore diameters up to 5.6 and 5.7 nm, respectively. The slight difference observed using distinct aluminum precursors may be attributed to the different organic-inorganic interfaces obtained during the templating pathway, allowing distinct chelation between Al atoms, carboxylic acids and Pluronic F127 moiety.[69] It could be also due to different density charge levels at these interfaces, allowing the self-assembly process in ethanol prior to the hydrolysis.[70] These pathways are governed by Van der Waals interactions, covalent and hydrogen bonding.[17]

BET analysis of the $ZnCl_2$-modified OMA showed a decreased BET surface area while pore volume and pore distributions are retained even upon pores filling by zinc chloride (Table 1). Therefore, it is suggested that this drop in BET surface is mainly due to additional calcination step (4 h at 400 °C) in comparison to the original OMA. Moreover, similar shifts were observed using other aluminum precursors (Table 1; see also Figure S2 in the Supporting Information).

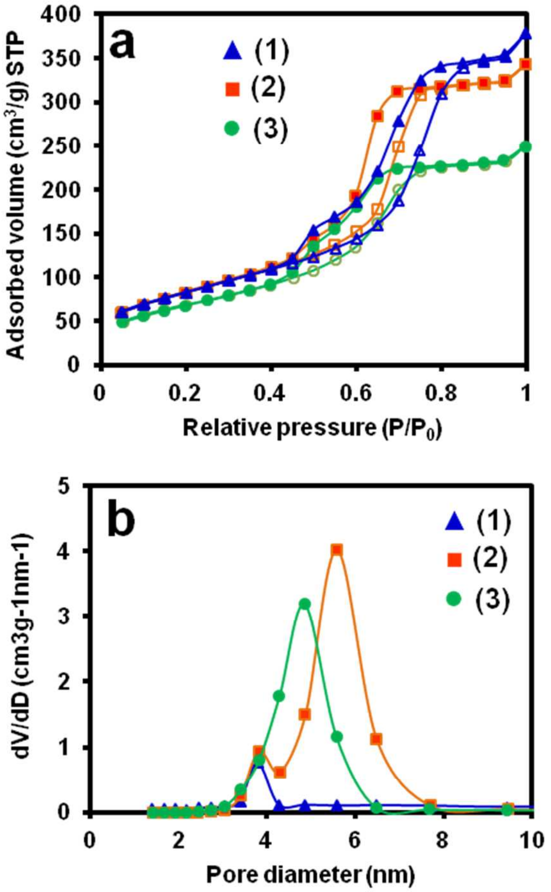

Fig. 2 (a) Nitrogen adsorption–desorption isotherms and (b) BJH pore size distributions curves of the prepared OMA samples using tartaric acid with different aluminum precursors: (1) Al_2O_3-$Al(NO_3)_3$•$9H_2O$, (2) Al_2O_3-$Al(OBu^t)_3$ and (3) Al_2O_3- $Al(OPr^i)_3$. All samples were calcined at 400 °C.

XRD analysis

Hexagonally mesostructured materials were successfully obtained as shown from small-angle XRD results in Figure 3a. The samples calcined at 400 °C exhibited three diffraction peaks (100, 110 and 200) at around 2θ = 1.0, 2.0 and 2.3°, respectively. This confirms the hexagonal mesostructure, which can be attributed to the *p6mm* space group.[23, 25] The formation of well-organized mesoporous network is confirmed by the high signal-to-noise ratio in small angle XRD patterns with narrow width at half-maximum of the (100) diffraction peak.

Zinc chloride modification did not result in any ordered mesostructure collapse, as shown in Figure 3b indicating similar patterns to those obtained with OMA materials.

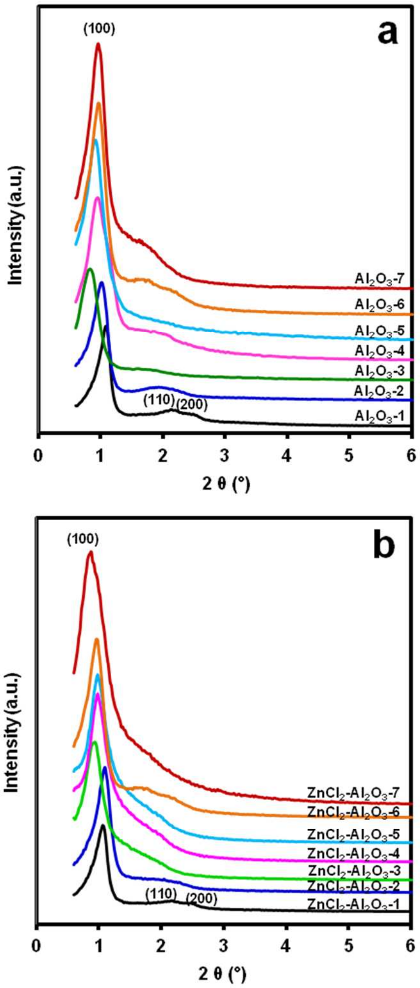

Fig. 3 Small-angle powder X-ray diffraction patterns for the prepared (a) ordered mesoporous alumina and (b) the zinc chloride-modified ordered mesoporous alumina synthesized using $Al(OBu^s)_3$ and calcined at 400 °C.

Small angle XRD patterns of $ZnCl_2$-modified OMA, prepared using other aluminum precursors exhibited similar diffraction peaks (Figure 4). However, the main diffraction peak at around 1.0° was slightly shifted to lower angles for the sample prepared with $Al(OPr^i)_3$ indicating the presence of relatively larger pore size.[71] This suggestion confirms the results of BET analysis.

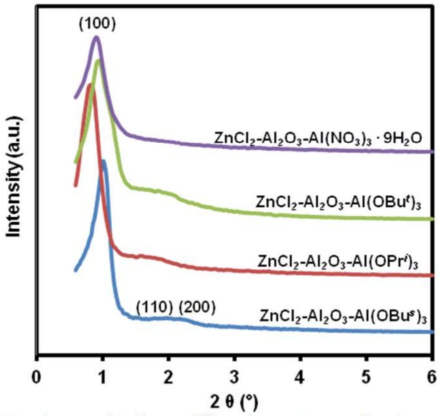

Fig. 4 Small-angle powder X-ray diffraction patterns for the prepared zinc chloride-modified ordered mesoporous alumina calcined at 400 °C using tartaric acid with different aluminum precursors.

Wide-angle XRD (WAXRD) patterns displayed in Figure 5 reveals the absence of any crystalline Al_2O_3 phase in the sample treated at 400 °C, suggesting that only amorphous network is formed. Moreover, further annealing at higher temperatures (800 °C) found to be sufficient to crystallize amorphous Al_2O_3 into the γ-Al_2O_3 phase as confirmed by wide-angle XRD patterns showing well-resolved diffraction peaks (111, 220, 311, 222, 400, 511 and 440) at around 2θ = 20, 34, 37, 39, 47, 62 and 77° . These peaks are assigned to the presence of γ- Al_2O_3 reflections (JCPDS Card, 10-0425). The presence of single γ-Al_2O_3 phase was observed with all the screened aluminum precursors. Surprisingly, this γ-Al_2O_3 phase remains stable even at elevated temperature up to 1000 °C, demonstrating the high thermal stability of these materials. However, under higher thermal treatment (1100 °C) conversion of γ-Al_2O_3 phase into α-Al_2O_3 phase (JCPDS Card, 11-0661) was observed.

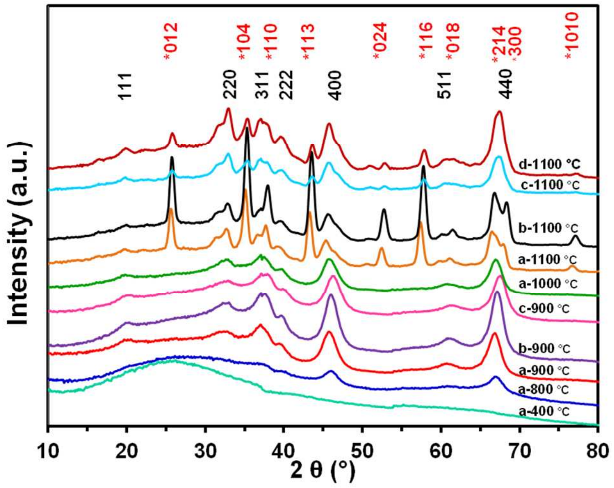

Fig. 5 Wide-angle XRD patterns of OMA samples calcined at different temperatures, prepared using citric acid with different aluminum precursors: (a) $Al(OBu^s)_3$, (b) $Al(OBu^t)_3$ and (c) $Al(OPr^i)_3$. Both γ-Al_2O_3 and α-Al_2O_3* phase diffraction peaks are indexed.

TEM analysis

In agreement with XRD measurements, the TEM images confirm that highly organized self-assembly process was achieved using the different carboxylic acids (Figure 6), revealing the hexagonal mesostructure and showing clearly the ordered mesoporous network aligned along [110] direction and arranged along [001] direction. Similar observations were portrayed in zinc chloride-modified OMA samples (see Figures S3 and S4 in the Supporting Information) in accordance with XRD results, confirming thus the maintained organized structure even after zinc chloride incorporation. It is worth to observe that the mean pore sizes as evaluated by TEM analysis are in the vicinity of 3 to 6 nm, confirming the mean pore sizes determined with BET analysis.

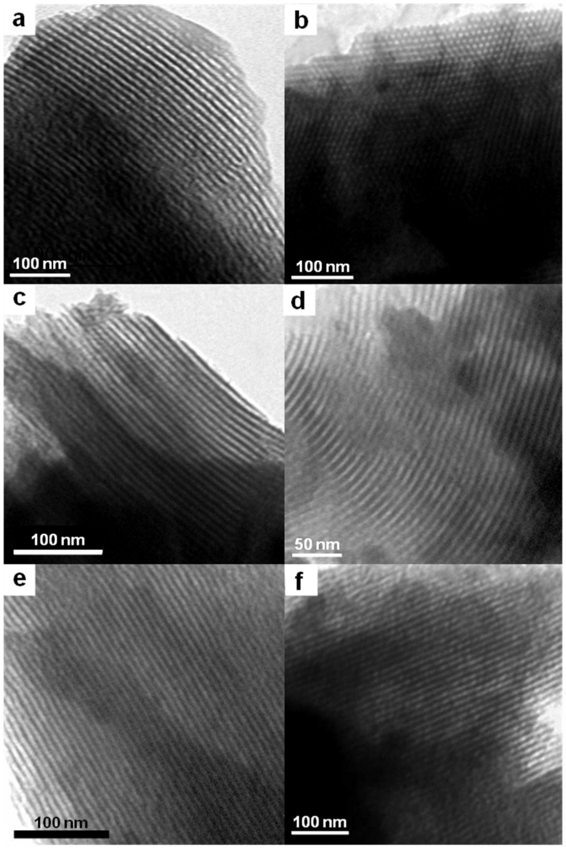

Fig. 6 TEM images of the synthesized ordered mesoporous alumina materials with different carboxylic acids; (a) citric, (c) fumaric, (d) malonic, (e) tartaric and (f) oxalic acid, viewed along [001] orientation and (b) maleic acid, viewed along [110] orientation.

SEM analysis

The SEM images displayed in Figure 7a highlight the microstructure of the non-uniform plate-shaped particles of the obtained OMA after template removal and crystal growth. The use of different carboxylic acids and several aluminum precursors did not result in any significant difference in the microstructure of the prepared OMA (Figures S5 and S6 in the Supporting Information). The SEM images display also the presence of microparticles which can be attributed to irregular aggregation of many nanoscale single crystals under thermal treatment. Moreover the microstructure observed with OMA was slightly modified after zinc chloride incorporation as depicted in Figure 7b (see also Figure S5 in the Supporting Information). The impregnation process allowed the formation of relatively smaller and less regular particle morphology and size. This can be observed in Figure 7b which shows medium-sized particles around 8-15 µm. It is believed that the presence of such smaller microparticles could be due to mechano-chemical dislocation effect during the $ZnCl_2$ incorporation process. The EDX spectrum of OMA sample displayed in Figure 7c exhibits only a strong signal for O and Al elements highlighting the evidence for mesoporous Al_2O_3 formation. Whilst, Au/Pd and C were also detected deriving from Au/Pd thin film used to enhance the sample surface electrical conductivity for better improved detection purpose and from the carbon film used for samples deposition, respectively. EDX analysis of $ZnCl_2$-modified Al_2O_3 samples depicted in Figure 7d shows also the presence of O and Al elements belonging to Al_2O_3 material. In addition, it shows the presence of both Zn and Cl elements owing to the impregnation of $ZnCl_2$ into to Al_2O_3 materials.

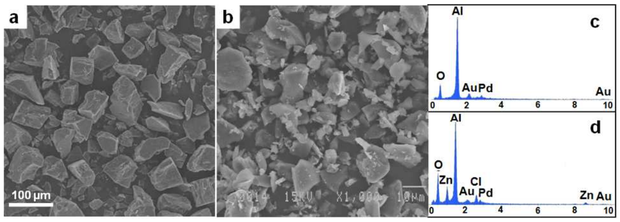

Fig. 7 Representative SEM images obtained for (a) OMA and (b) $ZnCl_2$-modified OMA microparticles prepared using oxalic acid with $Al(OBu^s)_3$. Energy dispersive X-ray (EDX) spectra of (c) OMA and (d) $ZnCl_2$-modified OMA samples prepared using oxalic acid-$Al(OBu^s)_3$.

XPS analysis

The XPS measurements of OMA samples confirmed the presence of only Al and O elements as depicted in the survey spectrum (Figure S7a in the Supporting Information) with the desired alumina stoichiometry having an Al:O atoms ratio close to 2:3. Al2*p* spectrum displayed in Figure 8a shows a strong signal at 74.3 eV binding energy, which is assigned to the Al element from the anhydrous amorphous alumina phase.[72] Moreover, all Al species (IV, V and VI) contribute to form the Al2*p* peak.[73] The deconvolution of O1*s* XPS spectrum of OMA samples reveals the presence of three different oxygen species on the bulk alumina (Figure 8b). The hidden signals were detected at 530.9, 532.1 and 533.1 eV, which are assigned to bulk oxygen from Al_2O_3 crystal matrix (Al-O-Al), the surface hydroxyl groups (Al-O-H) and the strongly adsorbed H_2O molecules, respectively.[60, 72] The presence of such moisture traces could be the reason behind the slight shift in the Al_2O_3 stoichiometry.

Figure 8d depicts the spectrum of Al2*p* peak of $ZnCl_2$-modified OMA at 74.7 eV. In comparison to the peak obtained for OMA material, the Al2*p* binding energy increased from 74.3 to 74.7 eV. This small shift could be attributed to the Al environment changes, especially surface hydroxyl groups that are modified with $ZnCl_2$.[72] However, this non-significant shift implies that all Al species on both OMA and $ZnCl_2$-OMA exhibit the same Lewis acidic properties.

On the other hand, similar O1*s* XPS spectrum was obtained for $ZnCl_2$-OMA samples (Figure 8c) without a significant shift, whilst lower intensities were observed for Al-O-H and H_2O signals. The estimated ratio of oxygen intensity in Al-O-Al over the oxygen in Al-O-H increased from ~ 2 (hexagonal mesoporous alumina) to ~ 3 ($ZnCl_2$-treated hexagonal mesoporous alumina). This may be due to the formation of Zn-O bonding as a consequence of $ZnCl_2$ interactions with Al-O-H species. Therefore, the occurrence of these species decreased after $ZnCl_2$ treatment of OMA. It is worth to note that was also suggested to be assigned to the formation of ZnO species resulted from the interaction of Zn with surface hydroxyl.[74] The H_2O low intensity signal is simply attributed to the second thermal treatment which helped to remove significant amount of moisture compared to bulk OMA.

The XPS analysis of $ZnCl_2$-promoted Al_2O_3 revealed the presence of Zn and Cl elements in addition to Al and O (Figure S7b in the Supporting Information). The expected nominal Al:Zn ratio of 8:1 is confirmed by ICP-OES analysis. However, the atomic element calculations resulted in Zn/Cl stoichiometry around 1.6 to 1.8. This statement could indicate that further to $ZnCl_2$, other Zn-Cl species are dispersed on the OMA surface as pointed out previously by Pillai *et al.* [55, 56]

Regarding the zinc element, Zn2$p_{3/2}$ XPS spectra displayed a unique signal at 1022.5 eV (Figure 8e). However, it is difficult to distinguish between different Zn^{2+} species since the presence of Zn^{2+} signal at this binding energy could be attributed to ZnO species (1022.5 eV)[75], $ZnCl_2$(1022.5 ±0.2 eV)[76] or $Zn(OH)_2$

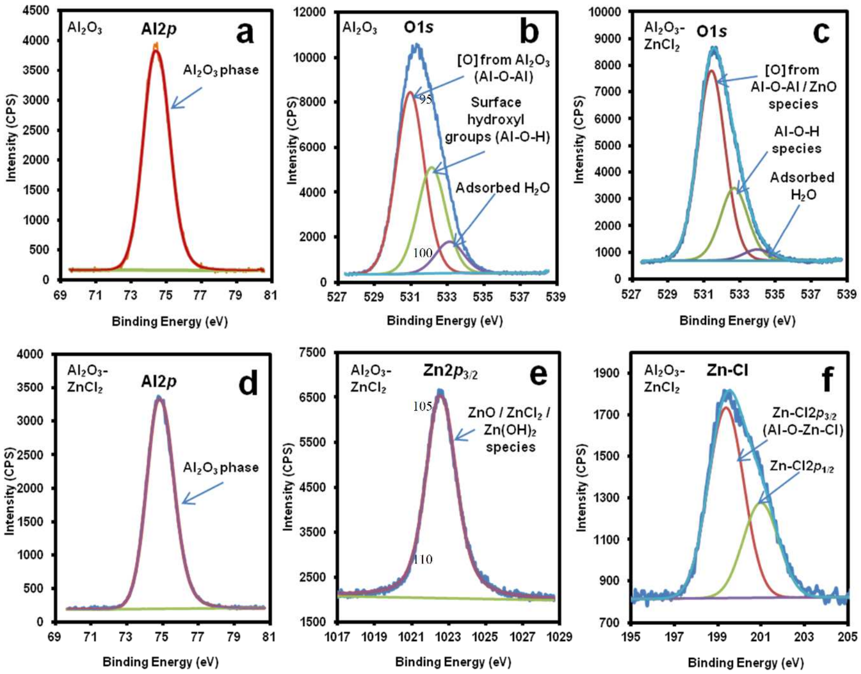

Fig. 8 XPS spectra of (a) Al2*p* and (b) O1*s* of the prepared OMA and (c) O1*s* and (d) Al2*p* (e) Zn2$p_{3/2}$ and (f) Cl2$p_{3/2}$ and Cl2$p_{1/2}$ of the zinc chloride modified OMA.

(1022.6 eV).[77] Nonetheless, it could be hardly assigned to a spinel $ZnAl_2O_4$ phase (1022.0 eV).[74] Therefore, the chlorine XPS spectra are necessary to confirm the nature of the related Zn^{2+} species. XPS spectrum of chlorine ions displayed in Figure 8f exhibits two signals at 199.3 and 200.9 eV for Cl2$p_{3/2}$ and Cl2$p_{1/2}$, respectively after peak deconvolution process. These signals are assigned to Cl bonded to Zn. The Zn-Cl species were also confirmed as Zn-Cl2$p_{3/2}$ with binding energy of 199.1 ± 0.2-0.9 and Zn-Cl2$p_{1/2}$ with a binding energy of 200.6 ± 0.2-1.462 eV. Moreover, the Zn-Cl2$p_{3/2}$ is suggested to be bonded to the alumina surface *via* OH groups as Al-O-Zn-Cl.[78] The calculated low Zn/Cl stoichiometry compared to the incorporated $ZnCl_2$ could be attributed to a partial removal of chlorine from the support surface upon zinc chloride decomposition under thermal treatment (400 °C) as reported recently by Schmidt *et al.*[79]

^{1}H and ^{27}Al –MAS-NMR Analyses

To confirm the presence of Zn-O-Al bond, ^{1}H-MAS-NMR analysis was conducted investigating the possible interaction of $ZnCl_2$ with the surface hydroxyl groups and the possible types of Zn/Cl species which can be obtained upon alumina modification. Recently, it was suggested that the incorporation of $ZnCl_2$ to alumina may lead to the formation of mixed Zn/O/Cl species, but the possible presence of bulk $ZnCl_2$ or elemental zinc is completely eliminated.[79]

First of all, the ^{1}H-MAS-NMR was conducted on OMA only and the results are depicted in Figure 9a which exhibit two main peaks observed at 1.7 and 3.8 ppm. These peaks can be assigned to the basic terminal hydroxyl groups and the acidic bridging hydroxyl groups of intermediate strength, respectively as it was previously reported by Decanio *et al.*[80] In contrast, strong acidic and basic hydroxyl groups were detected using wormhole-like alumina as reported in our previous work,[55, 56] as well as in other published results.[81] An additional peak was also observed at 4.3 ppm for OMA sample, which is assigned to hydrogen bonded water physisorbed on alumina surface.[80, 82] Afterwards, the $ZnCl_2$-modified OMA were analyzed and the results are reported in Figures 9b-9d. As depicted in these figures, the ^{1}H-MAS-NMR spectra reveal the elimination of the peak at 1.7 ppm. These observations suggest that the basic terminal hydroxyl groups are neutralized upon $ZnCl_2$ addition. It is believed that $ZnCl_2$ is bonded to the alumina surface *via* this type of hydroxyl groups forming various Al-O-Zn-Cl species; this was confirmed by combining the ^{1}H-MAS-NMR results with those obtained by XPS analysis. This neutralization leads to a drop in Brønsted acidity, and as a result an enhanced Lewis acidity of the catalyst support is obtained. The peak attributed to hydrogen bonded water physisorbed on alumina was observed also with $ZnCl_2$-modified alumina (Figure 9b). This peak was eliminated in other samples (Figures 9c-9d) which may be due to water trace removal *via* the second calcination process upon alumina modification.

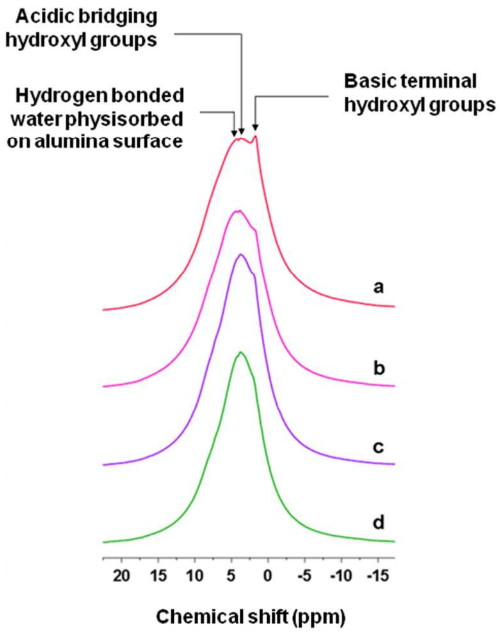

Fig. 9 ^{1}H-MAS-NMR spectra of (a) OMA prepared with oxalic acid-Al(OBus)$_3$. Zinc chloride modified alumina prepared with (b) oxalic acid-Al(OBu^s)$_3$, (c) tartaric acid-Al(OBu^t)$_3$ and citric acid-Al(OPr^i)$_3$. All samples were calcined at 400 °C.

Distinct shapes of the main signal were observed along with variation of carboxylic acid and aluminum precursors used for OMA and $ZnCl_2$-OMA synthesis. Decanio *et al.*[80] suggested that this signal broadening can be attributed to the strong ^{1}H-^{1}H dipolar interactions of the neighboring hydroxyl groups or physisorbed H_2O molecules. These ^{1}H-MAS-NMR results are supported by the DRIFT analysis reported previously by Tovar *et al.*[81] and in our previous work[55, 56] describing the disappearance of the terminal hydroxyl signals and decrease in bridging hydroxyl signals in the modified-wormhole-like alumina samples spectra in comparison to the initially analyzed wormhole-like alumina. Figure 10 shows the ^{27}Al-MAS-NMR spectra of as-prepared dried OMA and OMA calcined at 400 °C as well as $ZnCl_2$-modified OMA. Several carboxylic acids and aluminum precursors were screened for the preparation of these materials. The ^{27}Al-MAS-NMR spectra of the non-calcined (dried) samples exhibit a single peak centered at around $\delta = 0$ ppm which can be assigned to the octahedral Al-symmetry.[77] This was ascribed to the AlOOH intermediate phase.[83] The spectra of calcined materials exhibit tree major signals at around $\delta = 5$, 35 and 62 ppm compared to the as-prepared OMA, which are assigned to six-, five- and four-coordinated aluminum centers (Al^{3+}), respectively.[84] This was attributed to the enhanced dehydration and dehydroxylation upon calcination process.[58] All these peaks appear for both calcined and zinc chloride-modified OMA. However, compared to as-synthesized dried samples, calcined samples exhibit two new signals with high intensity for peaks at $\delta = 35$ (AlO_5) and 62.0 ppm (AlO_4) and lower intensity for the peak at 5.6 ppm (AlO_6). The origin of the observed conversion of octahedral Al-symmetry to pentahedral and tetrahedral ones could be due to the partial substitution of oxygen ions by hydroxyl groups in octahedral Al-centers during the template removal.[85, 86] Furthermore, the spectra of calcined OMA samples exhibit a relatively strong signal for Al penta-coordinated indicating higher content of AlO_5 centers. Fu *et al.*[87] related this phenomenon to the oxygen deficiency and distorted Al-O inside the alumina framework, as well as the substantial defects induced by relatively large surface area of the mesoporous networks.[88, 89] No significant difference on the distribution environment of Al centers was observed when using distinct aluminum precursors.

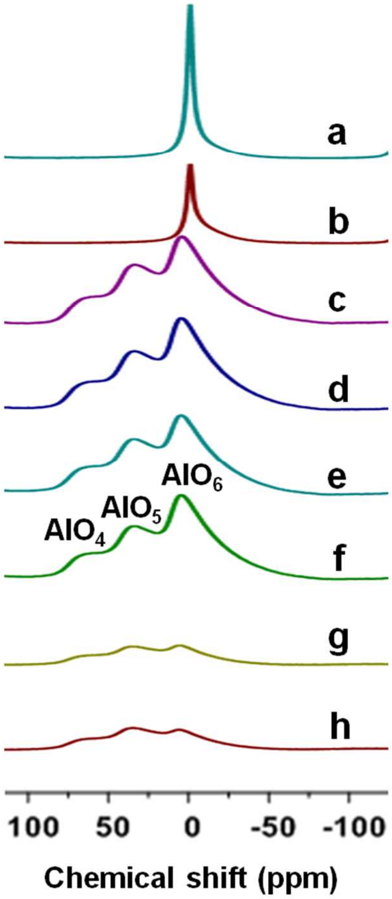

Fig. 10 ^{27}Al-MAS-NMR spectra of as-made OMA prepared using (a) citric acid-Al(OPri)$_3$ and (b) citric acid-Al(OBut)$_3$, and calcined OMA samples prepared using (c) citric acid-Al(OPr^i)$_3$, (d) citric acid-Al(OBu^t)$_3$, (e) tartaric acid-Al(OPr^i)$_3$, (f) tartaric acid-Al(OBu^t)$_3$, (g) oxalic acid-Al(OBus)$_3$ and (h) tartaric acid-Al(OBu^s)$_3$. All samples were calcined at 400 °C.

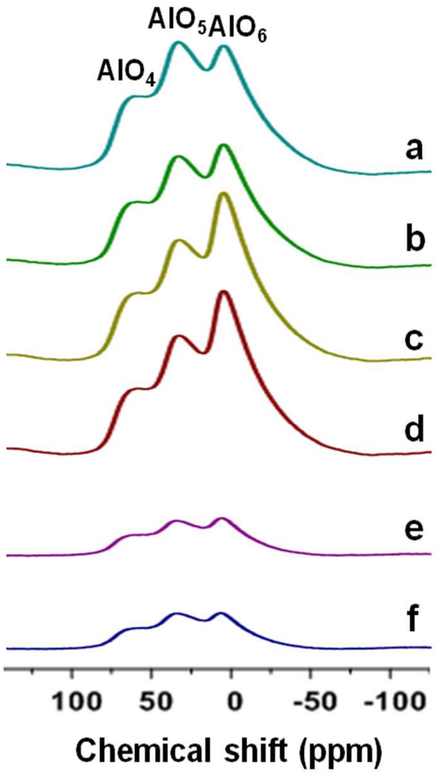

Fig. 11 ^{27}Al-MAS-NMR spectra of zinc chloride modified alumina synthesized using (a) citric acid-Al(OPr^i)$_3$, (b) citric acid-Al(OBut)$_3$, (c) tartaric acid-Al(OPr^i)$_3$, (d) tartaric acid-Al(OBu^t)$_3$, (e) oxalic acid-Al(OBu$^{s)}_3$ and (f) tartaric acid-Al(OBu^s)$_3$. All samples were calcined at 400 °C.

On the other hand, performing the synthesis in the presence of different carboxylic acids did not affect the Al coordination distribution for all OMA samples. In the case of zinc chloride-modified OMA, regardless of the Al precursor used, and for the samples using tartaric acid, the AlO$_5$ and AlO$_6$ distributions were conserved after zinc chloride incorporation (Figure 11). However, lower signal of AlO$_6$ was observed when citric acid was used. Surprisingly, this distribution was not observed with the corresponding unmodified OMA. It is believed that the tri-carboxylic acid (citric) led to higher amount of AlO$_6$ on OMA surface compared to the one prepared using the di-carboxylic acid (tartaric). This can be ascribed to the relative difference in the complexation ability of these acids with the Al precursors and bonding to the template before calcination process. It is then suggested that the difference on the exposed amount of AlO$_6$ can only be observed after zinc chloride incorporation upon interaction of Zn atoms preferably with AlO$_6$ coordination sites. Moreover, such selective doping was previously reported when Cu-doped Al$_2$O$_3$ was investigated showing high Cu atoms preference towards AlO$_5$ sites.[87] Therefore, the synthesized Al$_2$O$_3$ materials with high penta-coordinated aluminum distribution centers are highly desirable for heterogeneous catalysis.[87, 88]

Mechanism of OMA and ZnCl$_2$-modified OMA formation

In order to simplify the mechanistic pathway for the mesophase formation and based on well-established mechanisms and theories,[9, 10, 25, 89, 90] we propose herein a comprehensive mechanism for OMA synthesis and zinc chloride modification as schematically illustrated in Figure 12. In this mechanism, it is shown that the uniform aggregation of liquid-crystal phase of surfactant micelles is the main factor to be controlled in order to obtain such organized mesostructure. This agglomeration is obtained after a self-assembly process mediated by complexation effect of carboxylic acids with Al cations, as well as the nonionic surfactant (F127) *via* Van der Waals forces and hydrogen bonding[25] Therefore, carboxylic acids are used as interfacial protectors to prevent chlorine ions from complexation with Al atoms. Cl$^-$ anions can coordinate strongly with Al species leading the organized assemblies to collapse during the evaporation process.[25] Finally, the templating agent is removed upon calcination under 400 °C, providing the hexagonally structured mesoporous network.

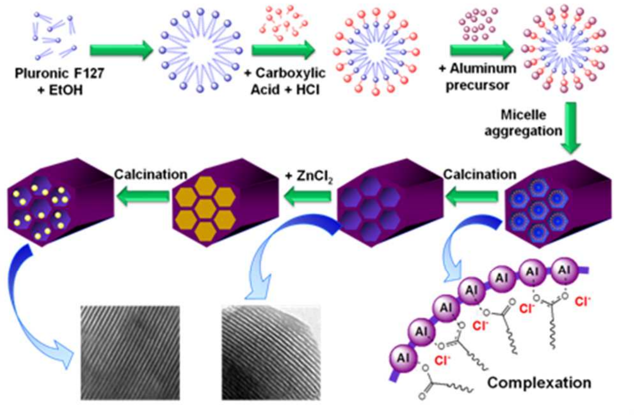

Fig. 12 Proposed mechanistic scheme for the formation of organized mesoporous alumina and zinc chloride-modified OMA.

ATR-FTIR analysis

ATR-FTIR measurements were conducted to verify and support the proposed mechanism involving the carboxylic acid-mediated mesophase formation and its interaction with aluminum metal centers. Figure 13 shows the ATR-FTIR spectra of both pure carboxylic acids and as-prepared alumina samples synthesized using different carboxylic acids and aluminum precursors. Pure citric and tartaric acid samples exhibit well-resolved signals at around 1728 and 1709 cm^{-1}, respectively. These bands are assigned to the carbonyl stretching vibration υ (C=O) of the free carboxylic acids. Moreover, for both acids, their spectra exhibit a second band at around 1677 and 1686 cm^{-1}, respectively. This band can be assigned to the H-bonded carbonyl stretching vibration υ (C=O) of the free carboxylic acids. Also, symmetric stretching vibrations $υ_s$ (COO$^-$) for free citric and tartaric acid are detected at around 1416 and 1443 cm^{-1}, respectively.[91] In the case of the as-synthesized alumina samples, they exhibit two new signals in addition to those observed for free citric acid, while the signal at around 1720-1740 cm^{-1} decreases, indicating the neutralization of citrate ions by Al atoms.[25] The newly appeared signals are assigned to the aluminum-coordinated citrate and tartrate groups: the increased signals at around 1438 and 1450 cm^{-1} are assigned υ (C=O) due to the monodentate coordination of citrate and tartrate groups to aluminum centers, respectively.[92] In addition, the spectra exhibit well-resolved bands at around 1590 and 1618 cm^{-1}, which are assigned to the asymmetric stretching vibrations $υ_a$ (COO$^-$) complexed to Al atoms.[91] These results demonstrate the evidence of carboxylic acid-Al coordination pathway leading to the mesophase formation and growth. These interactions are not tightly dependent on the nature of the carboxylic acid or the aluminum precursor.

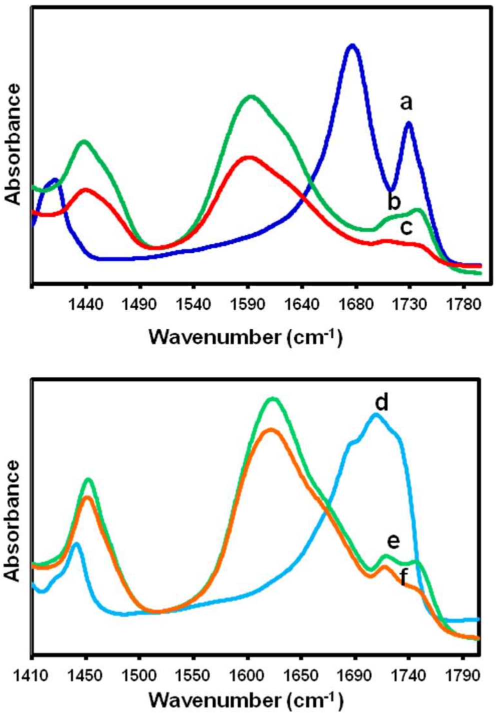

Fig. 13 ATR-FTIR absorbance spectra of (a) citric and (d) tartaric acid samples, and the as-prepared alumina samples synthesized using (b) citric acid-Al(OBu^t)$_3$, (c) citric acid-Al(OPr^i)$_3$, (e) tartaric acid-Al(OBu^t)$_3$ and (f) tartaric acid-Al(OPr^i)$_3$.

Catalytic activity for methyl oleate self-metathesis over heterogeneous MTO-based catalysts supported on organized mesoporous alumina

In order to evaluate the performance of the synthesized hexagonal mesoporous alumina materials as catalytic supports, some of the formulated MTO-based catalysts supported on these materials have been tested for their catalytic activity conducted on methyl oleate self-metathesis (See Scheme 1). The obtained results were also compared to those acquired using MTO catalyst supported on wormhole-like mesoporous alumina for the same reaction under identical reaction conditions (45 °C, 90 min of reaction time) as optimized previously by Pillai *et al.*[55, 56] These results are summarized in Table 2.

As already reported, the self-metathesis of methyl oleate with the MTO/ZnCl$_2$-Al$_2$O$_3$-meso catalyst gave the primary metathesis products 9-octadecene and dimethyl-9-octadecene-1,18-dioate in both *cis* and *trans* isomers. Methyl elaidate, which is the *trans*-isomer of methyl oleate, is also formed during the reaction. This product was obtained from the non-productive or degenerate metathesis as previously described.[55, 56, 93] It is worth to observe that when 3 wt% MTO supported on mesoporous alumina, unmodified with ZnCl$_2$ was used as catalyst, only weak methyl oleate conversion of 2.4% was reached after 3 h of reaction, testifying the poor catalyst performance: The yield of total metathesis products was 2.4% where only 43% of this yield is ascribed to the desired metathesis products (**1**, **2**, **4** and **5)**. The selectivity towards the desired products is in the vicinity of ~ 42%. The same catalyst modified with ZnCl$_2$ markedly boosted the conversion up to ~ 87% after the same reaction time where the

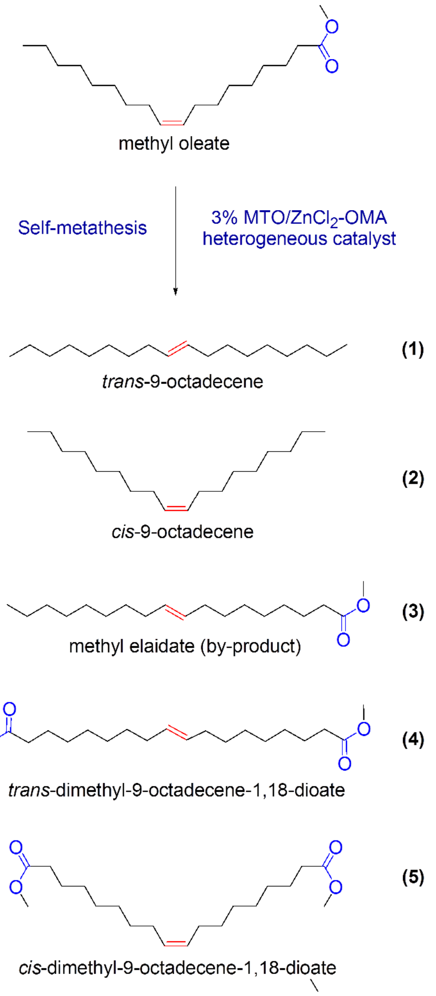

Scheme 1 Reaction pathway of methyl oleate self-metathesis.

Table 2 Catalytic activity for methyl oleate self-metathesis over heterogeneous MTO-based catalysts supported on organized or wormhole-like mesoporous alumina.

Catalyst[d]	**1**[a]	**2**[a]	**3**[a]	**4**[a]	**5**[a]	Conv[b]	DMP[c]	References
Cata #1	15.5	14.3	35.0	9.1	4.3	78.2	43.2	This work
Cata #2	29.3	8.5	32.9	12.9	4.6	88.2	55.3	This work
Cata #3	31.8	8.9	30.2	14.1	2.4	87.4	57.2	This work
Cata #4	24.4	8.3	34.3	16.2	3.6	86.7	52.4	Pillai *et al.*[55, 56]
Cata #5	0.2	0.3	1.4	0.2	0.3	2.4	1.0	Pillai *et al.*[55, 56]

[a] The numbers appearing for the metathesis products **1**, **2**, **3**, **4**, and **5** are expressed in terms of individual product yield (Yield$_i$), defined as: Yield$_i$ (%) = [Product$_i$]/([Methyl oleate]$_0$ –[Methyl oleate]$_t$)*100, where [Product$_i$] is the molar concentration of the product i =1 to 5, and [Methyl oleate]$_0$ and [Methyl oleate]$_t$ are the molar concentrations of methyl oleate initially and at a given time *t*, respectively. [b] Conv: Conversion, expressed as Conv (%) = ([Methyl oleate]$_0$ –[Methyl oleate]$_t$)/Methyl oleate]$_0$*100; [c] DMP: Desired metathesis products (**1**+**2**+**4**+**5**) yield which is represented by the summation of the individuals yields of **1**, **2**, **4** and **5**; [d] The investigated catalysts were 3 wt% MTO/ZnCl$_2$-Alumina-1, Alumina-2 and Alumina-11 in the case of **Cata #1**, **Cata #2** and **Cata #3**, respectively. **Cata #4** consisted of 3 wt% MTO on ZnCl$_2$-modified wormhole-like mesoporous alumina, while **Cata #5** was 3 wt% MTO on wormhole-like mesoporous alumina only.

total metathesis product yield attained 86.7% with 52% attributed to the desired metathesis products. This catalyst yielded also ~ 34% of methyl elaidate as reported in our previous work.[55, 56]

The MTO-based catalysts supported on some hexagonal alumina such as Al_2O_3-2 and -11 (Cata #2 and Cata #3, respectively) exhibited somewhat similar activity compared to the MTO-based catalyst supported on wormhole-like alumina. They reached comparable conversion. It is interesting to note that almost all these $ZnCl_2$-modified mesoporous alumina materials when they were tested as catalyst supports for methyl oleate self-metathesis, displayed almost similar conversion around 87 to 88% at identical reactions conditions. These catalysts were fairly more selective towards desired metathesis products. Their yield of desired products was slightly higher. This was reflected in somewhat lowering the non-productive metathesis product (methyl elaidate), indicating thus, a better selectivity towards the formation of the desired products. This statement is verified also in the next section treating the kinetics of the reaction.

Kinetic profiles of methyl oleate self-metathesis over MTO-based catalysts supported on $ZnCl_2$-modified mesoporous Al_2O_3

The activity and the products distribution yields of methyl oleate self-metathesis over MTO-based catalysts as shown in Table 2 were reached after 90 min of reaction. This long reaction time is considered sufficient to reach the chemical and thermodynamic reaction equilibria of methyl oleate self-metathesis. However, it is possible that this time would be finally shorter than can really appear in order to achieve such equilibria. In fact, for similar reaction conditions, this equilibrium time is dependent on how quick is the reaction for a given catalyst. This cannot be confirmed if a kinetic study is not carried out. For that purpose, the self-metathesis of methyl oleate is kinetically evaluated at the investigated temperature of 45 °C as depicted in Figure 14. It is clearly shown that the metathesis equilibrium was reached early far from 90 min of reaction for MTO-based catalysts supported on both types of $ZnCl_2$-modified mesoporous alumina where high methyl oleate conversions were obtained.

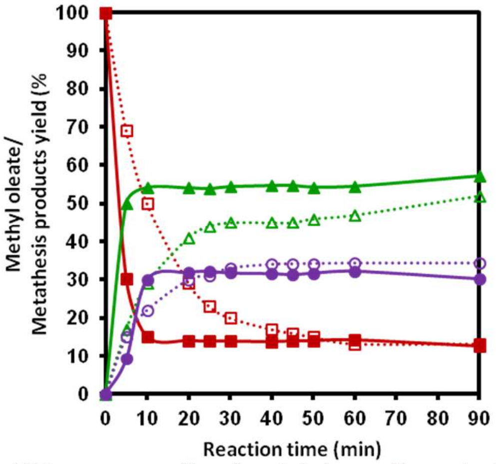

Fig. 14 Time-course profiles of methyl oleate self-metathesis over 3 wt% MTO/$ZnCl_2$-Al_2O_3 catalysts using highly ordered hexagonal and wormhole-like mesoporous Al_2O_3. Symbols: For ordered hexagonal Al_2O_3: ■ Methyl oleate; ▲ Desired metathesis products; ● Methyl elaidate. For wormhole-like Al_2O_3: □ Methyl oleate; Δ Desired metathesis products; ○ Methyl elaidate.

At the beginning of these equilibria, the yield of desired metathesis products attained 54% and 47% after 60 min of reaction when the catalysts were supported on hexagonal and wormhole-like mesoporous alumina, respectively. Moreover, with hexagonal alumina, the MTO-based catalyst seemed to be more selective towards desired metathesis products where only 30% of methyl elaidate, a non-productive metathesis product, was generated. Nevertheless, the time where the reaction begins to reach its equilibrium (onset equilibrium time) is much smaller (~10 min) when hexagonal alumina was used in comparison to wormhole-like structured alumina (30 to 40 min), indicating a huge activity of the MTO-based catalyst supported on hexagonally structured alumina which kinetically outperformed the MTO-based catalyst supported on wormhole-like structured alumina. Consequently, the new catalyst is more selective towards the desired products. Indeed, the products **1**, **2**, **4**, and **5** were formed *via* productive metathesis pathway, whereas the product **3** was formed *via* non-productive metathesis pathway which is a parallel unwanted side reaction. Frequently, the selectivity (*S*) can be defined as the yield of desired products over the yield of all undesired products. Then for the self-metathesis reaction, *S* can be evaluated by:

$$S = \frac{\text{Yield of desired metathesis products } (\mathbf{1}, \mathbf{2}, \mathbf{4} \text{ and } \mathbf{5})}{\text{Yield of the undesired metathesis product } (\mathbf{3})}$$

Table 3 summarizes this selectivity for both MTO-based catalysts using hexagonal and wormhole-like mesoporous aluminas.

Table 3 Selectivity towards the desired metathesis products for the heterogeneous MTO-based catalysts supported on hexagonal or wormhole-like mesoporous aluminas.

Catalysts	*S*
Cata #1	1.234
Cata #2	1.681
Cata #3	1.894
Cata #4	1.531
Cata #5	0.714

Therefore, it is evident that the MTO-based catalyst using hexagonal mesoporous alumina is more selective towards the desired metathesis products than that using wormhole-like alumina.

Even if the activity levels reached with both types of mesoporous alumina materials were quite similar, the kinetics was drastically improved with hexagonal mesoporous alumina compared to wormhole like alumina. In our opinion this could be attributed to the difference in the porous network structure of both alumina materials which greatly influenced the mass transfer phenomena, adsorption/desorption kinetics of the reactant (methyl oleate) as well as the desorption of the reaction products. In other words, in the case of wormhole-like structure, the reactant will take much more time to adsorb and react on the catalytic sites as well as the products to desorb from the catalyst pores. This is due to the irregular and interconnected porous network characterizing a wormhole-like framework structure, in comparison to the more regular hexagonal pores obtained with highly organized mesoporous alumina where the reactant and products diffusion inside the porous network, in addition to reactant adsorption on the catalyst sites and desorption of the products from the catalyst could be much easier and faster. The kinetics could be tightly dependent on the textural mesoporosity available for transporting substrates to the surface catalytic active sites. This suggestion corroborates that reported by Pauly *et al.*[94] when they studied the effect the textural mesoporosity and the catalytic activity of mesoporous molecular sieves with wormhole framework structures.

Conclusions

A successful preparation of hexagonal well-ordered mesoporous alumina and $ZnCl_2$-modified alumina in a simple, versatile, and reproducible process was carried out by a bottom-up approach through an evaporation-induced self-assembly technique, using Pluronic F127 and different carboxylic acids and aluminum precursors.

The synthesis allowed the formation of well-organized mesoporous alumina materials with moderate to relatively large BET surface areas and pore volumes, as well as interestingly uniform mesoporous network. Carboxylic acid and aluminum precursor choices are controlling parameters in this sol-gel synthesis. The complexation ability of carboxylic acids with Al centers is the key factor, leading to successful well-ordered assembly process. Zinc chloride enhanced greatly Lewis acidity of the supports, while mainly Al-O-Zn-Cl species are formed on the surface as illustrated with XPS and MAS NMR analysis. Theses ordered materials are potential candidates as catalysts supports for selective heterogeneous catalytic reactions, such as metathesis of functionalized bulky fatty molecules. The hexagonal alumina exhibited faster kinetics than those obtained with wormhole-like alumina counterpart. This behavior could be attributed to better mass transfer features of hexagonal mesoporous alumina. These finding and the synthesis reported herein are key points to elaborate a promising strategy for the synthesis and functionalization of various novel metal-doped organized supports. Moreover, they can pave the way to explore opportunities for the large-scale production of wide range of these interesting organized modified-mesoporous materials as catalytic supports.

Acknowledgments

The authors gratefully acknowledge the Natural Sciences and Engineering Research Council of Canada (NSERC) and Canadian Foundation for Innovation (CFI) who provided funds for this research. Alain Adnot, Pierre Audet and Richard Janvier are acknowledged for XPS characterization, MAS NMR analysis and TEM measurements, respectively. The authors thank Dr. K. T. Venkateswara Rao for his technical advices and for his kind suggestions during the early stages of this project.

Notes and references

1. C. Márquez-Alvarez, N. Žilková, J. Pérez-Pariente and J. Čejka, *Catal. Rev.*, 2008, **50**, 222-286.
2. X. Jiang, N. Suzuki, B. P. Bastakoti, K. C. W. Wu and Y. Yamauchi, *Chem. Asian J.*, 2012, **7**, 1713-1718.
3. B. P. Bastakoti, S. Ishihara, S.-Y. Leo, K. Ariga, K. C. W. Wu and Y. Yamauchi, *Langmuir*, 2014, **30**, 651-659.
4. X. Jiang, H. Oveisi, Y. Nemoto, N. Suzuki, K. C. W. Wu and Y. Yamauchi, *Dalton Trans.*, 2011, **40**, 10851-10856.
5. A. Taguchi and F. Schüth, *Microporous Mesoporous Mater.*, 2005, **77**, 1-45.
6. W. Li, Q. Yue, Y. Deng and D. Zhao, *Adv. Mater.*, 2013, **25**, 5129-5152.
7. D. Zhao, Y. Wan and W. Zhou, in *Ordered Mesoporous Materials*, Wiley-VCH Verlag GmbH & Co. KGaA, 2013, pp. 5-54.
8. L. Calvillo, V. Celorrio, R. Moliner, P. L. Cabot, I. Esparbé and M. J. Lázaro, *Microporous Mesoporous Mater.*, 2008, **116**, 292-298.
9. C. T. Kresge, M. E. Leonowicz, W. J. Roth, J. C. Vartuli and J. S. Beck, *Nature*, 1992, **359**, 710-712.
10. J. S. Beck, J. C. Vartuli, W. J. Roth, M. E. Leonowicz, C. T. Kresge, K. D. Schmitt, C. T. W. Chu, D. H. Olson and E. W. Sheppard, *J. Am. Chem. Soc.*, 1992, **114**, 10834-10843.
11. D. Zhao, J. Feng, Q. Huo, N. Melosh, G. H. Fredrickson, B. F. Chmelka and G. D. Stucky, *Science*, 1998, **279**, 548-552.
12. R. Schmidt, M. Stöcker and O. Henrik Ellestad, in *Studies in Surface Science and Catalysis*, eds. B. Laurent and K. Serge, Elsevier, 1995, vol. Volume 97, pp. 149-156.
13. F. Kleitz, S. Hei Choi and R. Ryoo, *Chem. Commun.*, 2003, 2136-2137.
14. R. Ryoo, S. H. Joo, M. Kruk and M. Jaroniec, *Adv. Mater.*, 2001, **13**, 677-681.
15. S. Jun, S. H. Joo, R. Ryoo, M. Kruk, M. Jaroniec, Z. Liu, T. Ohsuna and O. Terasaki, *J. Am. Chem. Soc.*, 2000, **122**, 10712-10713.
16. P. Yang, T. Deng, D. Zhao, P. Feng, D. Pine, B. F. Chmelka, G. M. Whitesides and G. D. Stucky, *Science*, 1998, **282**, 2244-2246.
17. P. Yang, D. Zhao, D. I. Margolese, B. F. Chmelka and G. D. Stucky, *Nature*, 1998, **396**, 152-155.
18. Y. Noda, B. Lee, K. Domen and J. N. Kondo, *Chem. Mater.*, 2008, **20**, 5361-5367.
19. G. J. d. A. A. Soler-Illia, C. Sanchez, B. Lebeau and J. Patarin, *Chem. Rev.*, 2002, **102**, 4093-4138.
20. S. Inagaki, S. Guan, T. Ohsuna and O. Terasaki, *Nature*, 2002, **416**, 304-307.
21. Y. Yamauchi, N. Suzuki and T. Kimura, *Chem. Commun.*, 2009, 5689-5691.
22. H. Oveisi, X. Jiang, M. Imura, Y. Nemoto, Y. Sakamoto and Y. Yamauchi, *Angew. Chem. Int. Ed.*, 2011, **50**, 7410-7413.
23. K. Niesz, P. Yang and G. A. Somorjai, *Chem. Commun.*, 2005, 1986-1987.
24. Q. Liu, A. Wang, J. Xu, Y. Zhang, X. Wang and T. Zhang, *Microporous Mesoporous Mater.*, 2008, **116**, 461-468.
25. Q. Yuan, A.-X. Yin, C. Luo, L.-D. Sun, Y.-W. Zhang, W.-T. Duan, H.-C. Liu and C.-H. Yan, *J. Am. Chem. Soc.*, 2008, **130**, 3465-3472.
26. Q. Wu, F. Zhang, J. Yang, Q. Li, B. Tu and D. Zhao, *Microporous Mesoporous Mater.*, 2011, **143**, 406-412.
27. F. Huang, Y. Zheng, G. Cai, Y. Zheng, Y. Xiao and K. Wei, *Scripta Mater.*, 2010, **63**, 339-342.
28. F. Huang, Y. Zheng, Y. Xiao, Y. Zheng, G. Cai and K. Wei, *Mater. Lett.*, 2011, **65**, 244-246.
29. Q. Sun, Y. Zheng, Z. Li, Y. Zheng, Y. Xiao and G. Cai, *Mater. Lett.*, 2012, **84**, 44-47.
30. X.-L. Zheng, Q.-P. Sun, F. Liu, Y. Zheng and J.-B. Weng, *J. Porous Mater.*, 2014, **21**, 819-825.
31. Z. Ramli and R. Saleh, *AIP Conf. Proc.*, 2009, **1136**, 26-30.
32. S. M. Grant and M. Jaroniec, *J. Colloid Interface Sci.*, 2012, **367**, 129-134.
33. S. M. Grant and M. Jaroniec, *J. Mater. Chem.*, 2012, **22**, 86-92.
34. S. M. Grant, A. Vinu, S. Pikus and M. Jaroniec, *Colloids Surf., A*, 2011, **385**, 121-125.
35. S. M. Morris, P. F. Fulvio and M. Jaroniec, *J. Am. Chem. Soc.*, 2008, **130**, 15210-15216.
36. W. Cai, J. Yu, C. Anand, A. Vinu and M. Jaroniec, *Chem. Mater.*, 2011, **23**, 1147-1157.
37. X. Zhao, Y. Zheng, Y. Zheng, Y. Zhan and X. Zheng, *RSC Adv.*, 2014, **4**, 12497-12505.
38. Q. Sun, Y. Zheng, Z. Li, Y. Zheng, Y. Xiao, G. Cai and K. Wei, *Phys. Chem. Chem. Phys.*, 2013, **15**, 5670-5676.
39. F. Huang, Y. Zheng, Z. Li, Y. Xiao, Y. Zheng, G. Cai and K. Wei, *Chem. Commun.*, 2011, **47**, 5247-5249.
40. E. Moretti, M. Lenarda, L. Storaro, A. Talon, R. Frattini, S. Polizzi, E. Rodríguez-Castellón and A. Jiménez-López, *Appl. Catal., B*, 2007, **72**, 149-156.
41. Q. Sun, Y. Zheng, Y. Zheng, Y. Xiao, G. Cai and K. Wei, *Scripta Mater.*, 2011, **65**, 1026-1029.
42. Z.-X. Li, F.-B. Shi, L.-L. Li, T. Zhang and C.-H. Yan, *Phys. Chem. Chem. Phys.*, 2011, **13**, 2488-2491.
43. H. Oveisi, A. Beitollahi, M. Imura, C.-W. Wu and Y. Yamauchi, *Microporous Mesoporous Mater.*, 2010, **134**, 150-156.
44. L. Xu, H. Zhao, H. Song and L. Chou, *Int. J. Hydrogen Energy*, 2012, **37**, 7497-7511.
45. Y. Bang, S. J. Han, J. G. Seo, M. H. Youn, J. H. Song and I. K. Song, *Int. J. Hydrogen Energy*, 2012, **37**, 17967-17977.
46. L. Kaluža, M. Zdražil, N. Žilková and J. Čejka, *Catal. Commun.*, 2002, **3**, 151-157.
47. T. Xiu, J. Wang and Q. Liu, *Microporous Mesoporous Mater.*, 2011, **143**, 362-367.
48. M. A. R. Meier, J. O. Metzger and U. S. Schubert, *Chem. Soc. Rev.*, 2007, **36**, 1788-1802.
49. A. H. Hoveyda and A. R. Zhugralin, *Nature*, 2007, **450**, 243-251.
50. J. C. Mol, *Green Chemistry*, 2002, **4**, 5-13.
51. R. H. A. Bosma, G. C. N. Van Den Aardweg and J. C. Mol, *J. Organomet. Chem.*, 1983, **255**, 159-171.
52. R. Spronk and J. C. Mol, *Appl. Catal.*, 1991, **76**, 143-152.
53. R. Buffon, A. Choplin, M. Leconte, J. M. Basset, R. Touroude and W. A. Herrmann, *J. Mol. Catal.*, 1992, **72**, L7-L10.
54. R. Buffon, A. Auroux, F. Lefebvre, M. Leconte, A. Choplin, J. M. Basset and W. A. Herrmann, *J. Mol. Catal.*, 1992, **76**, 287-295.
55. S. K. Pillai, S. Hamoudi and K. Belkacemi, *Appl. Catal., A*, 2013, **455**, 155-163.
56. S. K. Pillai, S. Hamoudi and K. Belkacemi, *Fuel*, 2013, **110**, 32-39.
57. S. K. Pillai, A. Abidli and K. Belkacemi, *Appl. Catal., A*, 2014, **479**, 121-133.
58. E. P. Barrett, L. G. Joyner and P. P. Halenda, *J. Am. Chem. Soc.*, 1951, **73**, 373-380.
59. R. B. Anderson, *J. Catal.*, 1964, **3**, 50-56.
60. B. C. Lippens and J. H. de Boer, *J. Catal.*, 1965, **4**, 319-323.
61. J. T. Kloprogge, L. V. Duong, B. J. Wood and R. L. Frost, *J. Colloid Interface Sci.*, 2006, **296**, 572-576.
62. J. F. Moulder, W. F. Stickle, P. E. Sobol and K. D. Bomben, *Handbook of X-ray Photoelectron Spectroscopy: A Reference Book of Standard Spectra for Identification and Interpretation of XPS Data*, Physical Electronics, Perkin-Elmer Corp, 1992.
63. D. Briggs and P. Seah, *Practical Surface Analysis: Auger and X-ray photoelectron spectroscopy*, John Wiley & Sons, first edition 1983, second edition 1990.
64. D. A. Shirley, *Phys. Rev. B: Condens. Matter Mater. Phys.*, 1972, **5**, 4709-4714.
65. D. Fenzke, D. Freude, T. Fröhlich and J. Haase, *Chem. Phys. Lett.*, 1984, **111**, 171-175.
66. S. Hayashi and K. Hayamizu, *Bull. Chem. Soc. Jpn.*, 1989, **62**, 2429-2430.
67. R. J. Motekaitis and A. E. Martell, *Inorg. Chem.*, 1984, **23**, 18-23.
68. M. Kruk and M. Jaroniec, *Chem. Mater.*, 2001, **13**, 3169-3183.
69. G. J. d. A. A. Soler-Illia and C. Sanchez, *New J. Chem.*, 2000, **24**, 493-499.

70. Q. Huo, D. I. Margolese, U. Ciesla, P. Feng, T. E. Gier, P. Sieger, R. Leon, P. M. Petroff, F. Schuth and G. D. Stucky, *Nature*, 1994, **368**, 317-321.
71. T. Seki and M. Onaka, in *Advanced Nanomaterials*, Wiley-VCH Verlag GmbH & Co. KGaA, 2010, pp. 481-521.
72. J. van den Brand, P. C. Snijders, W. G. Sloof, H. Terryn and J. H. W. de Wit, *J. Phys. Chem. B*, 2004, **108**, 6017-6024.
73. R. Lizárraga, E. Holmström, S. C. Parker and C. Arrouvel, *Phys. Rev. B: Condens. Matter Mater. Phys.*, 2011, **83**, 094201.
74. B. R. Strohmeier and D. M. Hercules, *J. Catal.*, 1984, **86**, 266-279.
75. S. W. Gaarenstroom and N. Winograd, *J. Chem. Phys.*, 1977, **67**, 3500-3506.
76. R. D. Seals, R. Alexander, L. T. Taylor and J. G. Dillard, *Inorg. Chem.*, 1973, **12**, 2485-2487.
77. L. S. Dake, D. R. Baer and J. M. Zachara, *Surf. Interface Anal.*, 1989, **14**, 71-75.
78. G. E. Muilenbenger, *Handbook of X-Ray Photoelectron Spectroscopy: Perkin-Elmer Corporation Minnesota*, 1979.
79. S. A. Schmidt, N. Kumar, A. Shchukarev, K. Eränen, J.-P. Mikkola, D. Y. Murzin and T. Salmi, *Appl. Catal., A*, 2013, **468**, 120-134.
80. E. C. Decanio, J. C. Edwards and J. W. Bruno, *J. Catal.*, 1994, **148**, 76-83.
81. T. Tovar, S. M. Stewart and S. Scott, *Top. Catal.*, 2012, **55**, 530-537.
82. C. E. Bronnimann, I. S. Chuang, B. L. Hawkins and G. E. Maciel, *J. Am. Chem. Soc.*, 1987, **109**, 1562-1564.
83. C. Boissière, L. Nicole, C. Gervais, F. Babonneau, M. Antonietti, H. Amenitsch, C. Sanchez and D. Grosso, *Chem. Mater.*, 2006, **18**, 5238-5243.
84. J. F. Stebbins, *Handbook of Physical Constants, V. 2; Ahrens, T. J., Ed.; American Geophysical Union: Washington DC*, 1995.
85. J. A. Wang, X. Bokhimi, A. Morales, O. Novaro, T. López and R. Gómez, *J. Phys. Chem. B*, 1998, **103**, 299-303.
86. J. Čejka, *Appl. Catal., A*, 2003, **254**, 327-338.
87. L. Fu, X. Li, M. Liu and H. Yang, *J. Mater. Chem. A*, 2013, **1**, 14592-14605.
88. H. J. Kim, H. C. Lee and J. S. Lee, *J. Phys. Chem. C*, 2007, **111**, 1579-1583.
89. M. Liu and H. Yang, *Colloids Surf., A*, 2010, **371**, 126-130.
90. J.-L. Blin, A. Léonard, Z.-Y. Yuan, L. Gigot, A. Vantomme, A. K. Cheetham and B.-L. Su, *Angew. Chem. Int. Ed.*, 2003, **42**, 2872-2875.
91. P. C. Hidber, T. J. Graule and L. J. Gauckler, *J. Am. Ceram. Soc.*, 1996, **79**, 1857-1867.
92. D. A. Thornton, *Coord. Chem. Rev.*, 1990, **104**, 173-249.
93. A. Salameh, A. Baudouin, J.-M. Basset and C. Copéret, *Angew. Chem. Int. Ed.*, 2008, **47**, 2117-2120.
94. T. R. Pauly, Y. Liu, T. J. Pinnavaia, S. J. L. Billinge and T. P. Rieker, *J. Am. Chem. Soc.*, 1999, **121**, 8835-8842.

Graphical Abstract

Synthesis, characterization and insights into stable and well organized hexagonal mesoporous zinc-doped alumina as promising metathesis catalysts carrier

Abdelnasser Abidli, [a,b] Safia Hamoudi [a,b] and Khaled Belkacemi* [a,b]

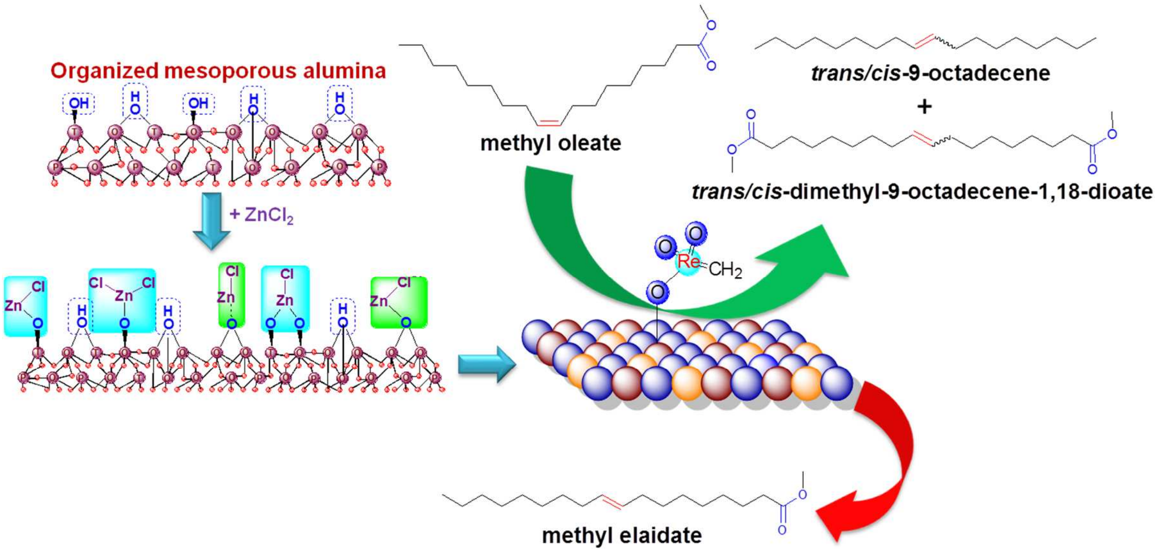

ZnCl$_2$-modified hexagonal mesoporous alumina was successfully synthesized, yielding Al-O-Zn-Cl species with promising properties for supporting MTO towards methyl oleate self-metathesis.